

# Deep-Trench Vertical Si Photodiodes for Improved Efficiency and Crosstalk

Yoshio Mita, *Member, IEEE*, Kenichiro Hirose, *Student Member, IEEE*, Masanori Kubota, *Member, IEEE*, and Tadashi Shibata, *Member, IEEE*

**Abstract**—The advancement of deep reactive-ion etching (DRIE) technology has enabled many 3-D structures, and are widely employed in microelectromechanical systems (MEMS). From an electrical point of view, however, those structures have been used as passive components such as capacitors and resistors. To further evolve the utility of future MEMS devices, the authors propose to integrate “active electrical devices” into 3-D MEMS. As an example, vertical trench photodiodes were fabricated on an n-type bulk silicon wafer using DRIE and thermal diffusion of boron. A photocurrent increase from 25% to 70%, and 20% smaller crosstalk was seen in 40-mm deep-trench diodes, as compared to a planar diode made on the same wafer.

**Index Terms**—Deep reactive-ion etching (DRIE), photo detector, thermal diffusion, trench diode.

## I. INTRODUCTION

DEEP reactive-ion etching (DRIE) technology appeared in the mid-1990s and, at present, plays an essential role in the fabrication of modern microelectromechanical systems (MEMS) fabrication. Typical usages of deep vertical structures are found in an optical fiber cross-connector application developed by Marxer *et al.* [1]: comb drive electrostatic actuators, springs, and optical components. From an electrical point of view, they can be classified either as passive components (i.e., capacitors) or nonelectrical components (i.e., mechanical). Robertson made a resistive matrix heater on the wall of DRIE through holes [2], which is also a passive device. Many 3-D active electrical devices have already been proposed in this area [3], but to the authors’ knowledge, no application of vertical active devices to the optical MEMS application has yet been reported. Therefore, it would be fair to say that the conventional use of MEMS silicon vertical wall is either as mechanical or as electrically passive components.

To further evolve the utility of future MEMS devices, the authors propose to integrate “active electrical devices” into 3-D MEMS (Fig. 1). Photodiode is one of the examples of active device [4]. Using a vertical photodiode, many novel photonic systems will become possible. A vertical photo detector for optical fiber interface is one of the examples (Fig. 2).

In this paper, the authors report fabrication and measurement of deep-trench vertical photodiode. Vertical trench photodiodes

Manuscript received October 2, 2006; revised October 27, 2006. This work was supported in part by a Semiconductor Technology Academic Research Center (STARC) grant-in-aid and in part by the Japan Society of Promotion of Science (JSPS) under Grant 17760274.

The authors are with the Intelligent Semiconductor Microdevices Laboratory (ISML), Department of Electrical and Electronics Engineering, University of Tokyo, Tokyo 113-8656, Japan (e-mail: MEMS@else.k.u-tokyo.ac.jp).

Digital Object Identifier 10.1109/JSTQE.2006.893078

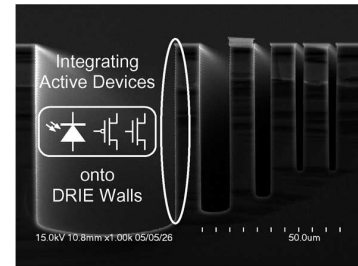


Fig. 1. Proposed new paradigm of deep-etched MEMS is to integrate active devices onto DRIE walls.

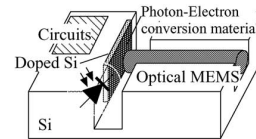


Fig. 2. Vertical photodiode integrated optical MEMS will be possible.



Fig. 3. Conventional planar (left) and trench (right) photodiode. A vertical photodiode can have three merits.

were fabricated on an n-type bulk silicon wafer using DRIE and thermal diffusion of boron. This novel valley-shaped photodiode achieved higher conversion efficiency (photocurrent), compared to the planar photodiode whose area is equal to that of deep vertical photodiode. Crosstalk was also evaluated, and trench diode showed lower crosstalk than planar diode.

## II. ADVANTAGES OF DEEP-TRENCH PHOTODIODE

Fig. 3 shows a schematic view of a conventional planar photodiode and deep-trench photodiode. As shown in the figure, there are three merits over planar photodiode: 1) junction area is larger in trench diode; 2) light can enter into trench; and 3) electron-hole collection depth is deep. All those advantages contribute to photocurrent increase and crosstalk suppression.

### A. Junction Area

Photocurrent in diode refers to the flow of electron and hole pair generated by incident light and accelerated by reverse bias to the p-n junction. The more the junction area is exposed to incident light, the more the current flows. Deep-trench diode has a larger junction area for a given top-view surface area as compared to planar diode.

### B. Light Propagation Into Trench

Incident light to a planar surface of silicon reflects, and reflected light does not contribute to the photocurrent. Conventional devices put antireflection coating on the surface to put as much light as possible into silicon. Trench diode is one of the ideal devices because light can enter into a trench. The incident light entering into the trench can reflect in between trench sidewalls, and will eventually be absorbed. For example, if reflection rate (reflected light power divided by incident light) is 30% [5], planar diode can receive only  $(1 - 0.3) = 70\%$  of incident light; if the light reflects three times in the trench, recoverable power of trench diode is  $(1 - 0.3) + 0.3 \times (1 - 0.3) + (0.3)^2 \times (1 - 0.3) = 97.3\%$ .

### C. Electron–Hole Collection Depth

It is known that electron–hole pair generated outside the p-n junction can flow into the junction and can also contribute to the photocurrent. Those pairs flow by diffusion, so that one cannot orient the direction of the flow, and electron may reach their adjacent and next adjacent p-n junction. For image sensor application, the electron–hole pairs reaching adjacent (and next adjacent) cells will cause crosstalk.

It is also known that light can enter very deep into silicon. Light diffusion is intuitively understood by the fact that when thinning a silicon wafer below  $10\ \mu\text{m}$ , the wafer gets transparent and color turns brown, which shows that red light is diffusing into silicon by  $10\ \mu\text{m}$ . Consequently, electron–hole pairs are also generated very deep in silicon.

Trench photodiode is also ideal to avoid crosstalk because the trench as deep as light diffusion depth can physically block the electron–hole. This is the same principle as a shallow-trench isolation technique in modern electron devices, but trench photodiode has an additional feature: Crosstalk current is suppressed by active absorption by diode, and absorbed current contributes to the photosensor output.

## III. DESIGN AND FABRICATION

Twenty-eight sets of trench diodes having  $0.6\text{--}100\ \mu\text{m}$  of width, all having  $100\ \mu\text{m}$  of length, and  $40\ \mu\text{m}$  of depth for large width are fabricated on an n-type 4-in bulk silicon wafer (resistivity:  $5\text{--}10\ \Omega\cdot\text{cm}$ ). Each trench diode had a planar diode adjacent to it for comparison. The process sequence is really simple: 1) DRIE; 2) boron diffusion; and 3) electrode formation.

The key issue of deep-trench photodiode is lithography near deep trench after etching. Fig. 5 shows a typical cross-sectional view of resist coated over trench that is deeper than resist

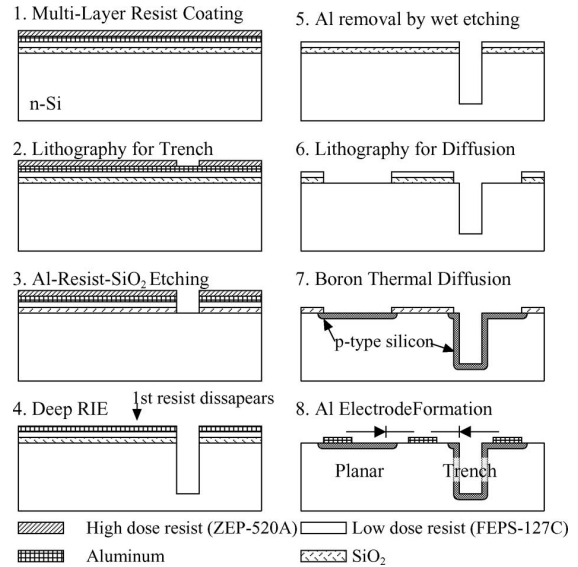


Fig. 4. Fabrication of deep-trench photodiode by planar lithography. The key is to embed all critical masks before deep trench.

thickness. There are three typical phenomena: 1) resist erosion at the corner of deep trench; 2) resist swelling at the edge; and 3) bubbles in trench. Those three phenomena make resist coating and lithography as near as  $10\ \mu\text{m}$  from trench edge too tricky, even though there exists some workarounds such as spray coating and electroplated resist. For the trench photodiode, the problem is crucial because oxide diffusion mask must be patterned after DRIE as near as  $1\ \mu\text{m}$  from the trench edge (step 6 in Fig. 4).

To overcome the lithography problem, the authors applied a planar lithography method on sandwiched electron beam resists. The guiding principle is called “embedded-masking-methods” [6]; all critical resist layers are embedded on the wafer before DRIE, and are used subsequently. In the case of trench diode, there are two critical layers: deep-trench Al mask and boron diffusion  $\text{SiO}_2$  mask. All critical layers with resist are embedded in the beginning of the process:  $\text{SiO}_2$ , high-dose resist, aluminum, and low-dose resist.

Fig. 4 shows the fabrication process of trench diode. An n-type 4-in silicon wafer (thickness:  $525\ \mu\text{m}$ , resistivity:  $5\text{--}10\ \Omega\cdot\text{cm}$ ) covered with  $100\text{-nm}\ \text{SiO}_2$  is used. A higher dose electron beam (EB) resist (ZEP-520A, Nippon Zeon Co.) was spun on, followed by  $100\text{-nm}$  aluminum evaporation. On top of the aluminum, another lower dose EB resist (FEPS-127C, FUJI FILM Electronics Materials Co.) was spun on (Fig. 4 step 1). Then, the area of the deep trench is exposed on the FEPS-127C by production-quality rapid EB-lithography machine (ADVANTEST F5112+VD01.) and developed by its developer [2.38% tetramethyl ammonium hydroxide (TMAH)]. The acceleration voltage and dose were  $50\ \text{kV}$  and  $7\ \mu\text{C}/\text{cm}^2$ , respectively. This low dose, together with aluminum shield layer, did not affect higher dose EB resist underneath. Aluminum was also patterned by long development at the TMAH step; it does not limit other etching methods such as  $\text{H}_3\text{PO}_4$  or  $\text{Cl}_2 + \text{BCl}_3$  RIE.

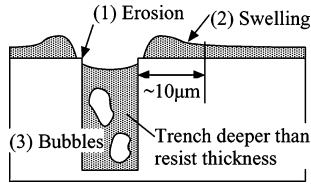


Fig. 5. Three issues that make resist coating after trench etching difficult.

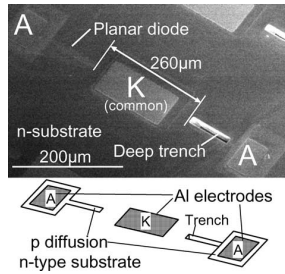


Fig. 6. Fabricated trench and planar diodes. They have a common cathode.

The wafer was deeply etched with a standard Bosch's process using inductively coupled plasma reactive-ion etching (ICP-RIE) apparatus. In the ICP-RIE step, the aluminum layer served as a hard mask (Fig. 4 steps 3 and 4). Embedded ZEP-520A and  $\text{SiO}_2$  at the trench were etched by ion bombardment of Bosch's process (self-alignment process). The reason of not having changed the etching recipe was for process simplicity, again not limiting other specialized process such as  $\text{O}_2$  ashing for resist and  $\text{CHF}_3$  RIE for  $\text{SiO}_2$ .

After DRIE, aluminum was removed by TMAH, and ZEP-520A was exposed by the EB writer ( $50 \text{ kV}$ ,  $100 \mu\text{C}/\text{cm}^2$ ) and developed by organic solvent-based developer (ZED-N50) to define the area to be doped.  $\text{SiO}_2$  was etched using buffered hydrofluoric acid (BHF16). During the DRIE process, ZEP-520A resist was exposed at the edge of deep trench. This resist recession at the edge of the trench was  $0.2\text{--}0.3 \mu\text{m}$  for 20 min of ICP-RIE. It did not affect doping area lithography, since doping area pattern implied whole trench.

Then, the whole wafer was cleaned by  $\text{O}_2$  plasma, followed by  $\text{H}_2\text{O}_2 + \text{H}_2\text{SO}_4$  (SPM) and  $\text{H}_2\text{O}_2 + \text{NH}_4\text{OH}$  (APM) to remove teflon from the trench.  $\text{O}_2$  ashing, twice as long as Bosch's process, sufficiently removed teflon from the trench.

Thermal diffusion is done with boron nitride planar diffusion source (BN-975, Saint-Gobain). Thermal diffusion is used to form the p-n junction on the vertical wall, because it is much more advantageous over other methods such as ion implantation that is severely limited by self-shadowing of deep trench [7]. After thermal diffusion,  $\text{SiO}_2$  film was removed by 50% hydrofluoric acid (HF). A very thin  $\text{SiO}_2$  was made by low-temperature ( $1025 \text{ K}$ ) thermal oxidation. This  $\text{SiO}_2$  layer was subsequently removed by HF, to remove the highly doped Si-B layer from the surface.

Aluminum electrode was deposited and patterned by photolithography using PFR-7790G (JSR Co.) (Figs. 4–8). Aluminum pattern was sufficiently large and far from deep trench,

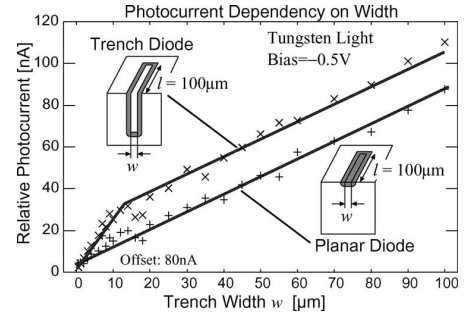


Fig. 7. Relative photocurrent as compared to the narrowest trench diode.

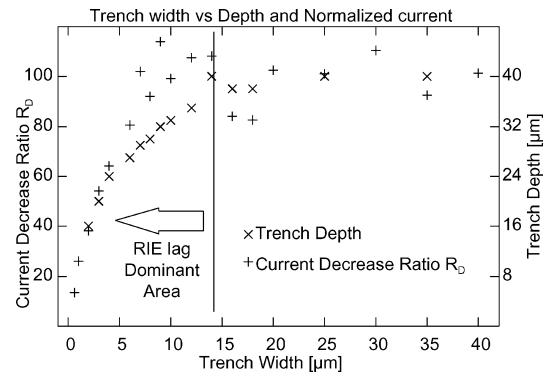


Fig. 8. Photocurrent decrease and trench-depth dependency on trench width.

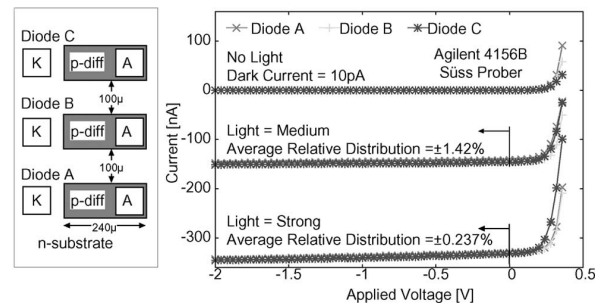


Fig. 9. Adjacent diodes have good matching.

so that conventional photolithography was possible. Trench re-filling is suggested, if finer lithography is needed for back-end process.

It should be noted that the authors have used EB resist and EB writer for two reasons: 1) EB resist is insensitive to room light and 2) light by evaporation and EB exposure time was sufficiently short for prototyping. Nominal exposure time for an entire 4-in wafer is less than 45 min. Of course, resist is not limited to EB resist. Suggested alternative combination is deep-UV resist, such as polymethylglutarimide (PMGI) for lower layer and normal photoresist for upper layer.

IV. PHOTOCURRENT INCREASE MEASUREMENT

Fig. 6 shows one of the prototype devices. The trench width, length, and depth are 20, 100, and 40  $\mu\text{m}$ , respectively. Tested 28 pairs of deep-trench and planar diodes are 100- $\mu\text{m}$  long and from 0.6 to 100  $\mu\text{m}$  wide. The distance between trench and planar diode is 260  $\mu\text{m}$ . Characteristics Current–Voltage ( $I-V$ ) are measured by semiconductor parameter analyzer (HP4156B, Agilent Technologies).

A. Trench Width and Photocurrent Increase

Fig. 7 shows relative photocurrent as compared to the photocurrent of the narrowest (0.6  $\mu\text{m}$ ) trench diode. Incident light was from a tungsten lamp of the probe station (Tokyo Seimitsu Co.), and applied reverse bias was  $-0.5$  V. Optical power was measured to be 10  $\text{mW}/\text{cm}^2$  by power meter ADVANTEST TQ8210 and 8-mm  $\phi$  sensor Q82014. Optical current increases as the width of trench and doped areas increases. Deep-trench photodiodes showed a conversion efficiency improvement from 25% to 70%. The largest current increase was found at  $w = 10\text{-}\mu\text{m}$  trench (14.9–25.4 nA). It was found that the larger the trench width was, the less important current increase became, for diodes over 10  $\mu\text{m}$ . The smallest current increase was measured for  $w = 100\text{-}\mu\text{m}$  trench (87.5–112 nA). The current increase saturation can be explained by the fact that contribution of trench wall becomes less important as compared to planar area.

It should be noted that all photodiodes had an offset current around 80 nA. Judging from relations between the trench and the other doped areas, this current is supposed to be generated around the electrode that has a large area of p-n junction (100  $\mu\text{m} \times 100 \mu\text{m}$ ). Since the target value of the measurement is relative increase of photocurrent at photodiode, the offset value is subtracted in Fig. 7. Dark current was less than 1 nA, which means that the current was less than 1 nA when the tungsten lamp was turned off.

B. Trench Depth and Photocurrent Increase

Photocurrent dependency on trench depth is examined by the measurement shown in Fig. 7. Trenches having width of less than 10  $\mu\text{m}$  was etched shallower than 40  $\mu\text{m}$ , which is the value of larger trench diodes. This phenomenon is widely known as “RIE lag” [8], or “aspect ratio dependent etching (ARDE)” [9], [10]. Because of that, junction area for narrower trenches decreased; thus, a current decrease was found.

Fig. 8 shows dependency current decrease ratio and etched trench depth on the trench width. Current decrease ratio  $R_D$  was measured by

$$R_D = \frac{I_{\text{real}}}{I_{\text{fit}}} \quad (1)$$

where  $I_{\text{real}}$  is a measured current value of trench diode and  $I_{\text{fit}}$  is a calculated value by least square fit from trenches of 10–100  $\mu\text{m}$ . Extracted linear fit function is

$$I_{\text{fit}} = 0.9493w + 16.127[\text{nA}](R^2 = 0.9893). \quad (2)$$

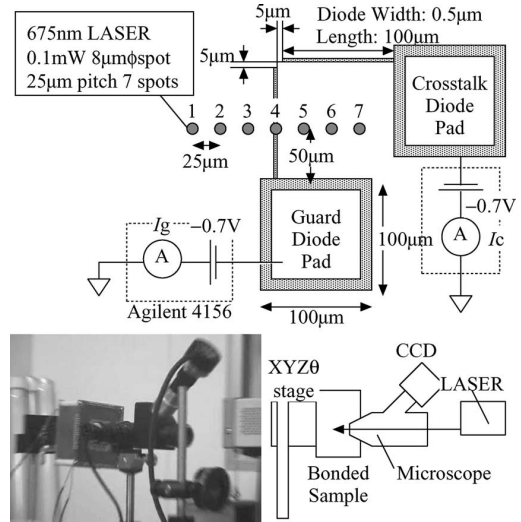


Fig. 10. Crosstalk measurement environment. The figure scales approximately.

Current decrease ratio  $R_D$  clearly agreed with etching depth decrease by RIE lag. This suggests a strong dependence of photocurrent increase on the trench depth.

C. Photocurrent Matching Between Adjacent Identical Diodes

To verify that the photocurrent increase was due to trench structure, not by chance of photocurrent fluctuation between devices, photocurrent of three adjacent planar diodes having identical shape (100  $\mu\text{m} \times 240 \mu\text{m}$ ) with spacing of 100  $\mu\text{m}$  were measured. These devices were made on the same wafer with trench diode (1–2mm apart). As clearly shown in Fig. 9, those photodiodes had a very small distribution from  $\pm 0.237\%$  to  $\pm 1.42\%$ . Taking the fact that the distance between trench diode and planar diode was 260  $\mu\text{m}$ , the current increase shown in Fig. 8 is attributable to the deep-trench device itself, not by haphazardness of process fluctuation.

V. CROSSTALK IMPROVEMENT MEASUREMENT

As shown in Fig. 10, two adjacent diodes were inversely biased at  $-0.7$  V by Agilent 4156B. One diode is called “guard diode” and the other is called “crosstalk diode.” They are sequentially exposed by seven 675-nm 0.1-W laser beam spots of 8  $\mu\text{m}$ . The beam spot was made by focusing semiconductor laser output by optical microscope. Current in each diode  $I_g$  and  $I_c$  are measured simultaneously. Then, ratio of each current ( $I_g$  and  $I_c$ ) to total current  $I_g + I_c$  is calculated. Total current was measured to be around 300 nA for planar diode and 60 nA for trench diode.

It is assumed that when spots are in between two diodes (spots 5, 6, and 7), photocurrent is shared by two diodes so that crosstalk suppression is weak. When the spot is at the opposite side of the crosstalk diode (spots 1, 2, and 3), on the contrary, major current flows into the guard diode so that crosstalk is suppressed.

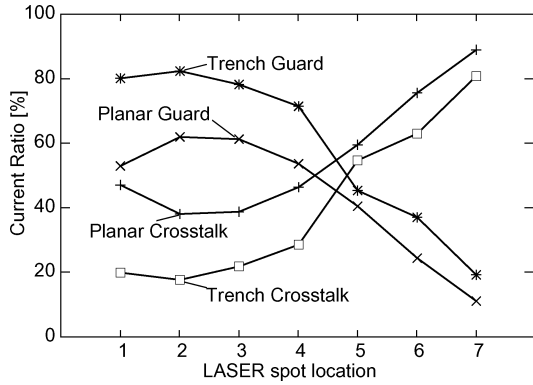


Fig. 11. Crosstalk is largely suppressed by trench diode. Maximum crosstalk suppression was 62% for planar diode and 82% for trench diode.

Fig. 11 shows the measurement result of planar and trench diodes with  $0.65\text{-}\mu\text{m}$  width and  $10\text{-}\mu\text{m}$  depth. Due to the availability of the samples,  $0.65\text{ }\mu\text{m}$  was chosen with which bonding wire did not shade laser spot. It is experimentally confirmed that crosstalk is suppressed in both devices. Maximum current ratio was found at spot 2 for both devices: 62% for planar diode and 82% for trench diode. Trench diode showed a better crosstalk suppression in the measurement.

At spot 4, the guard diode should ideally absorb all photocurrents, but which was not the case especially in planar diode. This phenomenon can be explained by the fact that focused red laser entered so deeply into the substrate that the light created a lot of electron-hole pairs outside the p-n junction.

## VI. CONCLUSION

A deep-trench photodiode was proposed towards active electrical device integrated optical MEMS. The key fabrication steps are very simple and consist only of DRIE and thermal diffusion of boron. In this process, a planar lithography method was employed. By "embedding" a couple of resist layers in the beginning and use them subsequently, fine lithography was ensured.

Increased current was measured for trench diodes depending on the trench width. Maximum current increase of 70% was measured for  $(w, d) = (10, 40)$  [ $\mu\text{m}$ ] trench diode. Larger crosstalk suppression by trench diode was also measured. For the sample of  $w = 0.65\text{ }\mu\text{m}$ , suppression ratio was 20% better for trench diode. Above results suggest an sensitive and fine-grained image sensors made by applied MEMS technology.

## ACKNOWLEDGMENT

An 8-in EB lithography system (F5112+VD01) was donated by ADVANTEST Corporation and belongs to the VLSI Design and Education Center (VDEC), University of Tokyo. Cadence Virtuoso layout editor was used through the academic program of VDEC. Alcatel ICP-RIE AMS-100 is proprietary of the 21st Century Center of Excellence Programs and maintained by Takeda Sentanchi Device Laboratory (AIMD). VAN partners Corporation is acknowledged by its FE-

SEM S-4700. Photoresist PFR-7790G was donated by JSR Corporation. Dr. Nakane and Mr. Sugiura are acknowledged for providing them with boron nitride planar diffusion source BN-975 donated by Saint-Gobain.

## REFERENCES

- [1] C. Marxer, C. Thio, M.-A. Grétilat, N. F. de Rooij, R. Bäattig, O. Anthamatten, B. Valk, and P. Vogel, "Vertical mirrors fabricated by deep reactive ion etching for fiber-optic switching applications," *IEEE J. Microelectromech. Syst.*, vol. 6, no. 3, pp. 277–285, 1997.
- [2] J. K. Robertson, "A vertical micromachined resistive heater for a micro-gas separation column," *Sens. Actuators A: Phys.*, vol. 91, no. 3, pp. 333–339, 2001.
- [3] C. Rochefort and R. van Dalen, "Vertical RESURF diodes manufactured by deep-trench etch and vapor-phase doping," *IEEE Electron Device Lett.*, vol. 25, no. 2, pp. 73–75, Feb. 2004.
- [4] K. Hirose, Y. Mita, M. Kubota, and T. Shibata, "Deep-trench vertical Si photodiode towards active-device integrated OMEMS," in *Proc. IEEE/LEOS Int. Conf. Opt. MEMS*, Big Sky, MT, Aug. 20–23, 2006, pp. 191–192.
- [5] S. H. Zaidi, D. S. Ruby, and J. M. Gee, "Characterization of random reactive ion etched-textured silicon solar cells," *IEEE Trans. Electron Devices*, vol. 48, no. 6, pp. 1200–1206, Jun. 2001.
- [6] Y. Mita, M. Mita, A. Tixier, J.-P. Gouy, and H. Fujita, "Embedded-mask-methods for mm-scale multi-layer vertical/slanted Si structures," in *Proc. 13th Annu. Int. Conf. Micro Electro Mech. Syst.*, Miyazaki, Japan, Jan. 23–27, 2006, pp. 300–305.
- [7] R. Kakoschke, R. E. Kaim, P. F. H. M. van der Meulen, and J. F. M. Westendorp, "Trench sidewall implantation with a parallel scanned ion beam," *IEEE Trans. Electron Devices*, vol. 37, no. 4, pp. 1052–1056, Apr. 1990.
- [8] H. Jansen, M. de Boer, R. Wiegink, N. Tas, E. Smulders, C. Neagu, and M. Elwenspoek, "RIE lag in high aspect ratio trench etching of silicon," *Microelectron. Eng.*, vol. 35, no. 1–4, pp. 45–50, 1997.
- [9] M. Francou, J. S. Danel, and L. Peccoud, "Deep and fast plasma etching for silicon micromachining," *Sens. Actuators A: Phys.*, vol. 46–47, pp. 17–21, 1995.
- [10] A. A. Ayon, R. Braff, C. C. Lin, H. H. Sawin, and M. A. Schmidt, "Characterization of a time multiplexed inductively coupled plasma etcher," *J. Electrochem. Soc.*, vol. 146, no. 1, pp. 339–149, 1999.



**Yoshio Mita** (S'96–M'00) received the B.Sc., M.Sc., and Ph.D. degrees in electrical engineering from the University of Tokyo, Tokyo, Japan, in 1995, 1997, and 2000, respectively.

Since 2005, he has been an Associate Professor in the Department of Electrical Engineering, University of Tokyo. His current interests include VLSI integrated microelectromechanical systems, and nanoscale and nanodevice fabrication by semiconductor technology.



**Kenichiro Hirose** (S'06) received the B.Sc. degree from the University of Tokyo, Tokyo, Japan, in 2006, where he is currently working toward the M.Sc. degree.

He received the MicroMechanics and Microengineering Europe 2006 Best Poster Award as the first author.



**Masanori Kubota** (M'07) received the B.Sc. and M.Sc. degrees from the University of Tokyo, Tokyo, Japan, in 2004 and 2006, respectively, where he is working toward the Ph.D. degree.

He is currently a Research Associate with the University of Tokyo. His current research interests include nanostructure fabrication technology.

Mr. Kubota received the MicroMechanics Europe 2005 Best Poster Award as the first author.



**Tadashi Shibata** (M'79) received the B.S. degree in electronic engineering and the M.S. degree in material science from Osaka University, Osaka, Japan, and the Ph.D. degree from the University of Tokyo, Tokyo, Japan, in 1971, 1973, and 1984, respectively.

He is currently a Professor in the Department of Frontier Informatics, University of Tokyo, Tokyo, Japan. He was with Toshiba Corporation as a VLSI Device and Manufacturing Engineer for 12 years. He proposed the concept of multiple-input floating-gate MOS device (neuron MOS) in 1991 and developed

various circuits using it. His current interests include developing intelligent VLSI systems based on the psychological brain model using state-of-the-art silicon technology.